PCCP

Molecular dynamics study of wetting of alkanes on water: From high temperature to the supercooled region and the influence of second inflection points of interfacial tensions

Journal:	*Physical Chemistry Chemical Physics*
Manuscript ID	CP-ART-03-2021-001108.R1
Article Type:	Paper
Date Submitted by the Author:	29-May-2021
Complete List of Authors:	Neupane, Pauf; Missouri University of Science and Technology, Department of Physics Wilemski, Gerald; Missouri University of Science and Technology, Department of Physics

SCHOLARONE™
Manuscripts

PCCP

ARTICLE TYPE

Molecular dynamics study of wetting of alkanes on water: From high temperature to the supercooled region and the influence of second inflection points of interfacial tensions[†]

Pauf Neupane[*] and Gerald Wilemski[*]

To explore the wetting behavior of alkanes on bulk water interfaces, molecular dynamics (MD) simulations were carried out for united-atom PYS alkane models, and for SPC/E and TIP4P/2005 water models over a wide temperature range. The MD results at each temperature were used to find (1) the surface tension of the alkanes (octane, nonane) and water, and (2) the interfacial tensions of the alkane-water systems. These quantities were then used to calculate the spreading coefficient (S) and contact angle (θ_c) for each alkane on water. At higher temperatures, the contact angle of octane and nonane on water is found to behave in accord with conventional expectations, i.e., it decreases with increasing temperature for both water models, as each system approaches the usual high-temperature transition to perfect wetting. At lower temperatures, we found an unusual temperature dependence of S and θ_c for each PYS alkane on SPC/E water. In contrast to conventional expectations, θ_c decreases with a decrease in the temperature. For octane-SPC/E water, this unusual behavior of θ_c occurs due to the presence of second inflection points (SIP) in the vapor-water and the octane-water interfacial tensions, whereas the SIP effect is much less important for the nonane-water system. The unusual temperature dependence of θ_c observed for nonane on SPC/E water is also found for nonane on TIP4P/2005 water. On the other hand, such unusual wetting behavior has not been observed in the PYS octane-TIP4P/2005 water system, except possibly for the two lowest temperatures studied.

1 Introduction

Aqueous organic systems play an important role in many environmental and industrial processes, such as the formation and growth of atmospheric aerosols, crude oil recovery from an oil-field, on-site cleaning of natural gas, and clean-up of oil spills. One of the common features underlying these processes is how well the water surface is wetted by the organic compound. When an oil droplet is present on the water surface in the presence of vapor, the wetting behavior is determined by the surface free energies, or equivalently the interfacial tensions. Usually, the sum of the interfacial tensions for the vapor-oil and oil-water interfaces exceeds that of the vapor-water interface, leading to the partial wetting of water by the oil droplet with a finite contact angle and a negative spreading coefficient. The spreading coefficient[1] is de-

fined as the following difference of the interfacial tensions:

$$S = \gamma_w - (\gamma_a + \gamma_{aw}), \tag{1}$$

where γ_w (γ_a) denote the surface tension of water (alkane) and γ_{aw} represents the alkane-water interfacial tension. The corresponding contact angle θ_c is defined by the rigorous thermodynamic formula[1]

$$\cos \theta_c = (\gamma_w^2 - \gamma_a^2 - \gamma_{aw}^2)/(2\gamma_a \gamma_{aw}). \tag{2}$$

Oil completely wets water when the vapor-water surface tension exactly balances the sum of the tensions of the remaining interfaces. In this case, we find $S = 0$ and $\theta_c = 0$ at the critical wetting transition temperature, T_w. The transition from partial to perfect wetting actually proceeds through several intermediate stages,[2–5] but here we are concerned only with the final transition to complete (or perfect) wetting. In principle, it is straightforward to determine the wetting state of water by another liquid using measured or computed values of the tensions to calculate S or θ_c, but there is a subtle complication, first noted by Gibbs,[6] in the proper use of Eq. 1 and Eq. 2. Although vapor-liquid surface tension values for pure alkanes (oil) and water are commonly available in the literature, what is actually required for wetting studies is

Department of Physics, Missouri University of Science and Technology, Rolla, MO 65409, USA.
E-mail: pndz2@mst.edu
E-mail: wilemski@mst.edu

the surface tension of each liquid fully saturated with the other liquid. [1] These values are rarely available, although there have been a few relevant studies of the adsorption of smaller alkanes on water and its effect on the surface tension. [7–10]

Moreover, experimental data on oil-water interfacial tensions and their temperature dependence are also quite limited. Goebel and Lunkenheimer, [11] and Mitrinović et al. [12] reported the interfacial tension of several alkane-water systems at a single temperature, as did Donahue et al., [13] and Rehfeld. [14] Matsubara et al. [9] studied the temperature dependence of the pentane-water interfacial tension. Aveyard and Haydon, [15] Mori et al., [16] and Zeppieri et al. [17] also studied the temperature dependent interfacial tension of several alkane-water systems, but it is difficult to obtain a high level of agreement among these studies. For example, the interfacial tension values in the latter six studies are consistently lower than those reported in Refs. [11,12] for the identical system and temperature, perhaps due to low levels of surface-active contaminants. Thus, the study of alkane-water wetting using experimental interfacial tension values is impractical due to the lack of appropriate or reliable interfacial tension data for a wide temperature range as just discussed. For a detailed example, see the ESI[†].

If one considers a computational approach to implement Eqs. (1) and (2), similar difficulties are encountered. While computational studies of surface tension are numerous, they also are largely limited to pure liquids with a few exceptions. [18,19] Many studies of water surface tension have been published using a variety of different models. [20,21] The temperature dependent surface tension for decane and the shorter alkanes has also been studied computationally, but to a lesser extent than water. [22–29] Similarly, relatively few molecular dynamics (MD) studies have considered the interfacial tensions of oil-water systems using various alkane/water models, [29–42] but many of these studies are at a single temperature or over a restricted range of temperature. It is also difficult to find models whose results are generally in close agreement with experiment. Moreover, even when nominally identical models are used, the published outcomes of such studies may differ because they depend upon key details of the simulations, such as system size, force field parameters, the cutoff range of the potentials, the simulation timestep and run time, and whether or not the results include the long range potential tail correction to the interfacial tension. In view of these factors, it is not feasible to conduct a study of wetting behavior from existing simulation results.

Experimental studies of temperature dependent wetting of alkanes on water are also scarce. A few studies have focussed on alkane behavior on water [16,43–46] and on aqueous ionic solutions. [47,48] All of these studies are consistent with a transition from partial wetting to perfect wetting at a higher temperature (T_w). Takii and Mori, [45] and Akatsuka et al. [46] showed that the spreading coefficients (S) of octane and shorter alkanes on water increase, i.e. become less negative, with increasing temperature. The negative S values below T_w correspond to the partial wetting of water by alkane. Rafaï et al. [48] experimentally studied the temperature dependence of the contact angle θ_c formed by hexane on brine, and found that θ_c decreases with increasing temperature

as T_w is approached. A similar temperature dependent behavior of θ_c was found theoretically for alkanes on water [49–53] and on brine. [50,51] On the other hand, Hrahsheh and Wilemski [54] found a highly unusual increase of θ_c with an increase in temperature in their MD simulations of nonane-water nanodroplets below 300 K. Such a positive correlation between the contact angle and the temperature is known to occur only for a pair of partially miscible liquids having a lower consolute temperature. [55,56] At and below the consolute temperature, the two liquids are miscible. Somewhat above the consolute temperature, the system undergoes a transition to perfect wetting.

Octane and nonane have very limited miscibility with water and no lower consolute temperature, so an increase of the contact angle with temperature is not expected. Consequently, we undertook the present study with two goals: (1) to ascertain whether or not the unusual behavior of the contact angle found in the nonane-water nanodroplets simulations would also be found in bulk systems and (2) to understand better how this unusual behavior depends on the molecular models used and, perhaps, on other details of the simulations. In particular, we seek to explore how the wetting of water is influenced by the "second inflection point" (SIP) in the water surface tension curve [57] and in the alkane-water interfacial tension curves computed here.

In this work, we use MD simulations to study the temperature dependent wetting behavior of octane and nonane on water. We determine the alkane-vapor, water-vapor, and alkane-water interfacial tensions at planar interfaces. The computed interfacial tension values are then used to calculate the spreading coefficients and contact angles formed by the alkanes on water. Due to system size and simulation time limitations, our simulated interfacial tensions have the same deficiency as the experimental tensions in that they are for pure liquids not equilibrated with the other liquid. As a result, our simulated values of S and θ_c are probably more representative of initial values, rather than full equilibrium values. [1] Finally, we also explore the effect of the potential cutoff radius on the interfacial tensions, and examine the significance for wetting behavior of long-range tail corrections to the interfacial tensions. We are unaware of any other study of temperature dependent wetting in alkane-water systems using MD techniques.

2 Simulation Details

To determine the temperature dependent interfacial tensions, the simulation systems were typically constructed as follows: (i) an alkane slab containing 620 octane molecules or 550 nonane molecules was placed at the middle of a rectangular box of cross-section of 5.5×5.5 nm^2 such that liquid occupies one third the volume of the box, (ii) a slab of 990 water molecules was kept at the middle of a rectangular box with volume $3.1 \times 3.1 \times 9.0$ nm^3, and (iii) a slab of 990 water molecules was sandwiched between a pair of identical alkane slabs, each containing 105 octane molecules or 100 nonane molecules. The cross-sectional area of the liquid-liquid simulation boxes was 3.1×3.1 nm^2, and the length of the box varied with temperature. All the dimensions were chosen to satisfy the minimum image criterion.

As in the previous work [54] on nonane-water nanodroplets, the alkanes were treated with a united-atom PYS (Paul-Yoon-Smith)

forcefield.[58–61] This model has been used to study crystallization and nucleation in bulk liquid alkanes,[59–61] freezing of alkane nanodroplets,[62] surface freezing of alkanes,[63] the orientations of alkanes at free and water interfaces during crystallization[41] and wetting in aqueous-organic nanodroplets.[54] Two rigid water models were studied: the popular SPC/E[64] model and the TIP4P/2005[65] model, which gives quite accurate surface tension values over a very wide temperature range. In addition to a Lennard-Jones interaction between each pair of water molecules, charged sites in the water molecules interact with Coulomb potentials. In the united-atom (UA) approximation for the alkanes, each carbon atom represents a single effective interaction site (C), and individual H-H interactions are ignored. The intermolecular interactions and the intramolecular interactions separated by four or more bonds were handled with a Lennard-Jones (LJ) potential

$$V_{LJ} = 4\varepsilon \left[\left(\frac{\sigma}{r}\right)^{12} - \left(\frac{\sigma}{r}\right)^{6} \right], \qquad (3)$$

where ε and σ are the LJ energy and size parameters, respectively. For oxygen-oxygen (O-O) interaction in water, $\varepsilon = 0.1553$ kcal/mol (SPC/E) or 0.1852 kcal/mol (TIP4P/2005) and $\sigma = 3.166$ Å (SPC/E) or 3.1589 Å (TIP4P/2005). The PYS model does not assign different interaction parameters for the methyl and methylene groups. For methyl (CH_3) or methylene (CH_2) interactions in PYS alkane, $\varepsilon = 0.112094$ kcal/mol and $\sigma = 4.01$ Å. In alkanes, the nearest neighbor UA-sites interact with bond stretching (V_b) and bond angle vibrating (V_a) potentials. Also included are torsional interactions[66] (V_t) for all groups of three consecutive sites. These potentials are given by the formulas

$$V_b = k_b (l - l_0)^2,$$
$$V_a = k_a (\theta - \theta_0)^2, \qquad (4)$$
$$V_t = \sum_{n=1}^{3} k_n \left[1 - \cos(n\phi) \right],$$

where l, θ and ϕ are the bond length, bond angle and the torsional angle, respectively. The equilibrium bond length l_0 is 1.53 Å and the equilibrium angle θ_0 is 109.526°. The bond stretching constant k_b is 349.0 kcal/mol Å^2, angle bending constant k_a is 60 kcal/mol rad^2, and the torsional constants are $k_1 = 0.7995$ kcal/mol, $k_2 = -0.4338$ kcal/mol and $k_3 = 1.6205$ kcal/mol.

The O-C interactions are also described by the LJ potential with the interaction parameters ε_{oc}, σ_{oc} optimized to roughly match the experimentally determined spreading coefficient (S) of alkane on water near 300 K. Since the computer models of pure water and alkanes do not reproduce experimental values of the surface tensions perfectly, we felt it preferable to match the S values rather than the liquid-liquid interfacial tensions with the hope of balancing the inaccuracies of the three interfacial tensions to achieve realistic predictions of wetting. If the usual Lorentz-Berthelot combining rules[67,68] are used for ε_{oc}, σ_{oc} for the alkane-SPC/E water interactions, we find the values $\varepsilon_{oc} = 0.55$ kJ/mol = 0.13194 kcal/mol, and $\sigma_{oc} = 0.36$ nm. As seen in Table 1, the S values obtained using these values in our simulations

Table 1 Comparison of spreading coefficient for alkane on water for different ε_{oc} ($\sigma_{oc} = 0.36$ nm)

Model	ε_{oc} (kJ/mol)	T (K)	S (mN/m)
octane-water			
Expt.		295	-1.5 [a, b, c]
Expt.		298	-1.0 [a, b, d]
PYS-SPC/E	0.55	300	-12.1
PYS-SPC/E	0.65	300	-1.2
PYS-TIP4P/2005	0.66	300	-1.9
nonane-water			
Expt.		295	-2.7 [a, b, c]
Expt.		298	-2.9 [a, b, d]
PYS-SPC/E	0.55	300	-14.9
PYS-SPC/E	0.65	300	-3.6
PYS-SPC/E	0.66	300	-2.7
PYS-TIP4P/2005	0.66	300	-4.7

[a] γ_w from Ref. [69], [b] γ_a from Ref. [70], [c] γ_{aw} from Ref. [11], [d] γ_{aw} from Ref. [12]

deviated greatly from the values determined using experimental interfacial tensions[11,12,69,70] near 300 K. These large discrepancies were reduced by suitably parameterizing ε_{oc}, keeping $\sigma_{oc} = 0.36$ nm. Unless otherwise stated, for alkane-water interactions our simulations used $\varepsilon_{oc} = 0.65$ kJ/mol (0.1554 kcal/mol) and 0.66 kJ/mol (0.1578 kcal/mol) for the SPC/E and TIP4P/2005 models, respectively. With these ε_{oc} and σ_{oc} parameters, the calculated S values near 300 K were found to be in much better agreement with values using experimental surface tensions than those based on the L-B combining rules.

All initial configurations were built using PACKMOL[71] and moltemplate[72] software. Simulations over a wide range of temperatures were performed with the LAMMPS[73] molecular dynamics simulation package. All the simulations were carried out in a canonical (NVT) ensemble for pure liquids and in a constant-NP_NAT ensemble[74] for the two-liquid systems, where P_N and A represent the normal pressure and the cross-sectional area, respectively. The value of P_N in the constant-NP_NAT simulations was chosen to be 1 atm for $T \leq 400$ K, and was increased for $T > 400$ K to exceed the water vapor pressure in order to prevent the vaporization of the liquids at the higher temperatures. Periodic boundary conditions were applied in all directions. The time step was set at 2 fs as explained in the ESI[†]. The equations of motion were solved using the velocity Verlet integrator.[75] After at least 2 ns of equilibration, the interfacial tensions were determined from 3-8, 20-40 ns long runs. To control the temperature, the Nosè-Hoover[76,77] thermostat was used with a coupling time constant of 0.2 ps. The pressure was controlled using a Parrinello-Rahman[78] barostat with a coupling time of 2.0 ps. The SHAKE algorithm[79] was used to keep the water molecule rigid. The electrostatic interactions were handled using a particle-particle particle-mesh (pppm) solver.[80]

At each temperature, the time-averaged density profiles were fitted to a hyperbolic tangent function[81]

$$\rho(z) = \frac{1}{2}(\rho_A + \rho_B) - \frac{1}{2}(\rho_A - \rho_B)\tanh\left(\frac{z - z_0}{d}\right), \qquad (5)$$

where ρ_A and ρ_B represent the density in the liquid phase and in the vapor phase, far from the interface, respectively for a vapor-liquid interface. For a liquid-liquid interface, $\rho(z)$ represents the

density profile of liquid A, with ρ_A and ρ_B being its densities in the liquid A rich region and in the liquid B rich region, respectively. In Eq. 5, z_0 represents the position of a Gibbs dividing surface, at which the density becomes half of the bulk value, and d is the interfacial thickness parameter which is related to the "10-90" thickness t as $d = t/2.1972$.[32] The interfacial tensions were determined by integrating the difference of the normal ($P_N(z)$) and tangential ($P_T(z)$) pressure components along the direction normal to the interfaces as

$$\gamma = \frac{1}{2} \int_{-\infty}^{\infty} dz [P_N(z) - P_T(z)]. \qquad (6)$$

Here, the factor of $1/2$ accounts for the presence of two such interfaces in our simulation cell. For our geometry, $P_N(z) = P_{zz}(z)$ and $P_T(z) = (P_{xx}(z) + P_{yy}(z))/2$.

The LJ interactions were truncated at $r = r_c$, and a long-range tail correction γ_t was added to the surface tension values as explained in the ESI[†]. The r_c values were chosen to be 1.5 nm for vapor-water and alkane-water simulations, and 1.75 nm for vapor-alkane simulations. The value of γ_t was calculated using the formula given by Chapela *et al.*[81] and later modified by Blokhius *et al.*[82] Following Li *et al.*[83] and Lundberg and Edholm,[84] the tail correction can be compactly expressed as

$$\gamma_t = 3\pi(\Delta\rho_D/r_c)^2 g_t(r_c/d), \qquad (7)$$

where g_t is a dimensionless integral that depends on r_c/d,

$$g_t(r_c/d) = \int_0^1 ds \int_0^1 dx\, x(3s^3 - s) \coth(s(r_c/d)/x), \qquad (8)$$

and where the dispersion density difference $\Delta\rho_D$ depends on the type of interface. For a vapor-liquid interface of molecules with only a single type of interaction site, it is given by

$$(\Delta\rho_D)^2 = 4\varepsilon\sigma^6(\rho_A - \rho_B)^2, \qquad (9)$$

and for a liquid-liquid interface it can be written generally as

$$(\Delta\rho_D)^2 = 4(\varepsilon_1\sigma_1^6\rho_1^2 + \varepsilon_2\sigma_2^6\rho_2^2 - 2\varepsilon_{12}\sigma_{12}^6\rho_1\rho_2), \qquad (10)$$

where ε_i, σ_i are the LJ parameters for site type i and ρ_i is its bulk density obtained from the simulated density profiles. The latter expression differs from those found in Refs. [83] and [84] because we explicitly avoid using the geometric mean approximation (GMA) for ε_{ij} and σ_{ij}. It is generally valid irrespective of the combining rules used for ε_{ij} and σ_{ij}, but it reduces to those results when the GMA is applied. Finally, the contact angles formed by alkane on water were calculated using Eq. 2.

3   Results

In this work, we report the temperature dependence of the interfacial tensions, and the temperature dependent wetting behavior of PYS alkanes (*n*-octane and *n*-nonane) on SPC/E and TIP4P/2005 water models.

3.1   TEMPERATURE DEPENDENCE OF THE INTERFACIAL TENSIONS

We studied the effect of temperature on the surface tension of water, alkane (octane, nonane), and on the alkane-water interfacial tension. To evaluate the long range tail correction γ_t, the interfacial thickness parameter d must be determined from the simulated density profiles. In Fig. 1, density profiles for SPC/E water and octane are plotted for 210 K, 350 K, and 400 K temperatures. Dashed lines and solid lines represent the fitted density profiles of water and octane, respectively, calculated using Eq. 5. For better statistics, the left half of the simulation box is mirrored and averaged with the right half during the calculation of the density profiles. It is noteworthy that at low temperatures, < 250 K but shown here only for 210 K, both the water and octane density profiles contain an apophysis, a high density, compact surface layer found in several recent studies for water,[85–87] and for PYS octane[63] and nonane.[41] Similar density profiles for the octane-SPC/E water system at temperatures 210 K and 400 K are shown in Fig. 2. Here, as well, there are apophyses in the water and octane density profiles at 210 K. The apophysis in the alkane profiles appears to be related to molecular ordering at the interface.[41] Similar results for nonane-water are shown in the ESI[†].

The surface tension of water has been extensively studied both experimentally and computationally. Hacker's experimental data
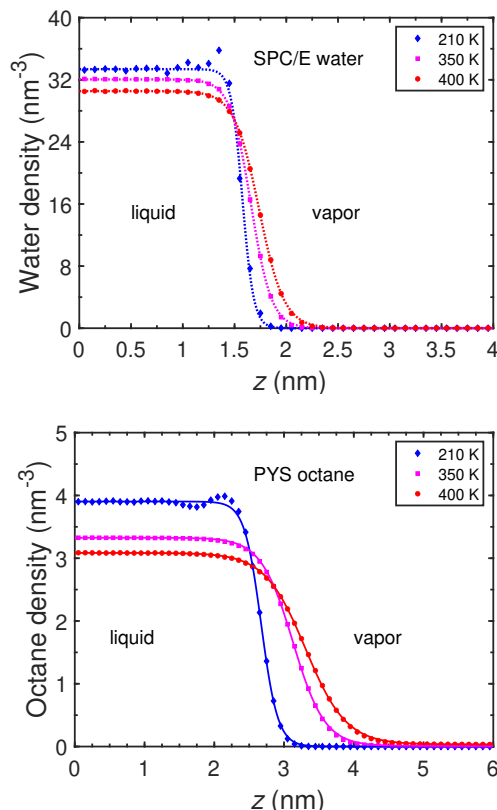

Fig. 1 Number density profiles of SPC/E water (upper) and PYS octane (lower) plotted for different temperatures. Points are the densities calculated using bin size of 0.1 nm. Dotted and solid lines represent the profiles fitted using Eq. 5.
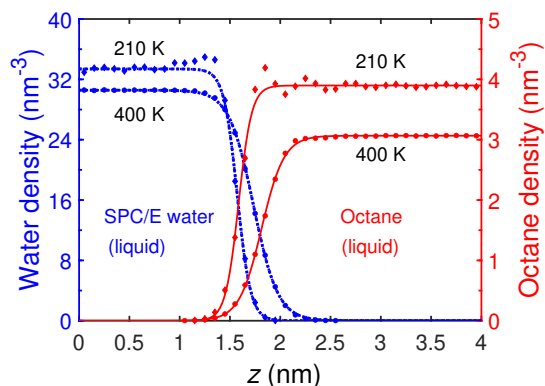
Fig. 2 Number density profiles of SPC/E water and PYS octane in the octane-water system at 210 K (diamonds) and at 400 K (circles) temperatures. Points are the densities calculated using bin size of 0.1 nm. The fitted profiles for water and octane are represented by the dotted and solid lines, respectively.

from 1951 show an anomaly in the surface tension of water at lower temperatures,[88] namely, the presence of a second inflection point (SIP) on the surface tension curve (in addition to the normal high temperature inflection point). In the supercooled region, where metastable liquid exists below the melting temperature (T_m), the surface tension was found to increase more rapidly with decreasing temperature due to the SIP. Based upon these data, Holten, Labetski, and van Dongen in 2005 had suggested a fit with a SIP at 267.5 K.[89] Subsequent experiments performed by Hrubỳ et al.[90] and Vinš et al.[91,92] showed no SIP in the water surface tension data measured down to 250 K. This situation has been dramatically altered by the very recent measurements of Vinš et al.[57] at even lower temperatures down to 241.8 K that provide support for the presence of the SIP in the water surface tension curve at temperatures below 253.2 K.

A number of different water models have been used to study the properties of water computationally. MD simulations of the surface tension for several of these models have been compared in Ref. [20,21]. A few simulations, performed at sufficiently low temperatures, have shown the presence of the SIP in the SPC/E and TIP4P/2005 water models.[87,93] The cause of the SIP in these models is not yet fully understood, but because the surface tension is sensitive to the local fluid density in the interfacial zone, Wang et al.[87] have suggested that the density apophysis predicted by these models may be a significant contributing factor.

Our simulation results for the surface tension of the SPC/E and TIP4P/2005 water models are in close agreement with the previous studies of these models[20,21,87,94–97] as seen in Fig. 3. Given the possibility of two inflection points on the surface tension curve, the computed surface tension values for the entire temperature range were fit to quartic equations to estimate the inflection temperatures. Based on these fits, the low temperature inflection points were determined to be at about 275 K (SPC/E) and 292 K (TIP4P/2005). Wang et al.[87] found the SIP of both SPC/E water and TIP4P/2005 water to lie in the temperature range of 240-250 K. This temperature region lies well above the melting temperature for SPC/E water (T_m = 213 K) and only
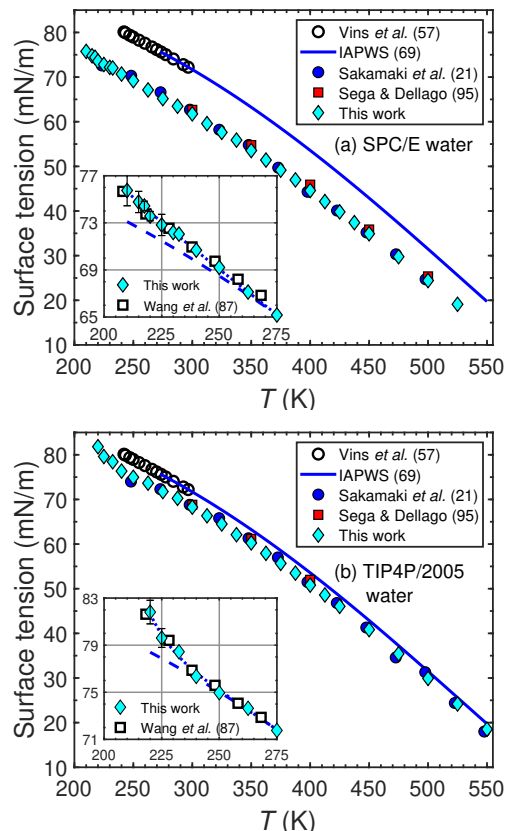

Fig. 3 Surface tension of (a) SPC/E water and (b) TIP4P/2005 water plotted as a function of temperature. Our results (diamonds) are compared with three previous studies.[21,87,95] The open circles and the solid lines represent experimental results.[57,69] In the inset, the dashed line represents the fitted surface tension obtained using Eq. 11, and the dotted line adds Eq. 12 to Eq. 11. The black error bars in the inset figures are the standard error of the mean.[98] They are shown only when they exceed the marker size. For a complete list of the standard errors, see Table S1-S4 in the ESI[†].

slightly below the melting temperature for TIP4P/2005 water (T_m = 249 K).[21] Given that T_m of SPC/E and TIP4P/2005 water differ greatly from the T_m of real water (273.15 K), we note that the SIP occurs in the stable liquid region for SPC/E water and in the slightly supercooled region for TIP4P/2005 water unlike in real water where it is found in the deeply supercooled region at about 20 K below the melting point.[57]

The surface tension values for temperatures above the SIP temperature (T_s) are correlated using the IAPWS functional form,[21,69,87,89] Eq. 11,

$$\gamma(T) = a\left(1 - \frac{T}{T_c}\right)^{11/9}\left[1 - b\left(1 - \frac{T}{T_c}\right)\right], \qquad (11)$$

where a, b, and T_c (critical temperature) are the fitting parameters. Here, we assume T_s = 275 K for both SPC/E water and TIP4P/2005 water. To accomodate the deviation of the simulated $\gamma(T)$ values from the low temperature extrapolation of the high temperature fit (Eq. 11), we add a function $\gamma^*(T)$ where, follow-
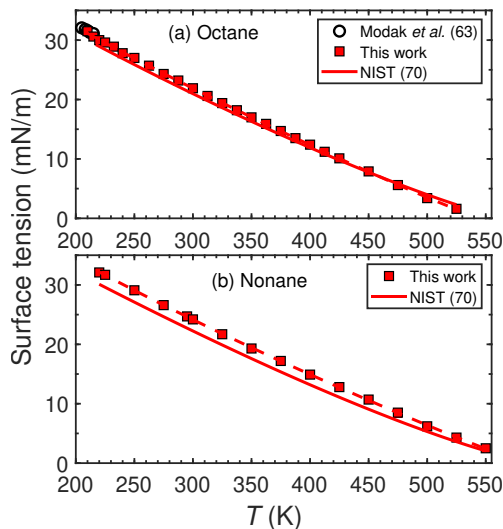
Fig. 4 Surface tension of (a) octane and (b) nonane plotted as a function of temperature. Our results (squares) are compared with NIST surface tension values (solid lines).[70] The dashed line represents fitted surface tension values using Eq. 13. Our PYS octane surface tension values agree well with a previous study performed at lower temperatures (circles).[63] All of the standard error of the mean are smaller than the marker size, and are not shown here.

ing Holten et al.,[89]

$$\gamma^*(T) = c'\left[\tanh((T_s - T_a)/T_b) - \tanh((T - T_a)/T_b)\right], T \leq T_s, \quad (12)$$

and c', T_a and T_b are fitting parameters. In the insets of Fig. 3, the surface tension values are shown for $T \leq T_s$. The dashed lines were obtained using Eq. 11, and would represent the surface tension if the SIP were not present in the surface tension curves. The dotted lines show the sum of Eq. 11 and Eq. 12. The simulated surface tension values at lower temperatures deviate increasingly from the dashed line with decreasing temperature. This behavior is consistent with the previously established SIP in the surface tension of the SPC/E[87,93] and TIP4P/2005[87] water models.

In Fig. 4, the surface tension of PYS octane and PYS nonane are plotted versus temperature and are compared with the respective NIST[70] surface tension values. The PYS octane results slightly overestimate the NIST surface tension values for $T < 450$ K, but they underestimate the NIST values for the two highest temperatures studied. On the other hand, the PYS nonane surface tension is consistently slightly larger than the NIST values. The alkane surface tension values were fit to the following equation[99]

$$\gamma_a(T) = a\left(1 - \frac{T}{T_c}\right)^{1.26}\left[1 - b\left(1 - \frac{T}{T_c}\right)^{0.5} + c\left(1 - \frac{T}{T_c}\right)\right], \quad (13)$$

with a, b, c, and T_c as fitting parameters.

The alkane-water interfacial tensions are shown in Fig. 5. Diamonds and circles represent simulation results, and the asterisk and star represent experimental alkane-water interfacial tensions from Ref. [11] and Ref. [12], respectively. All computed interfacial tensions at 300 K are lower than the experimental interfacial tension values, although the TIP4P/2005 results are much closer
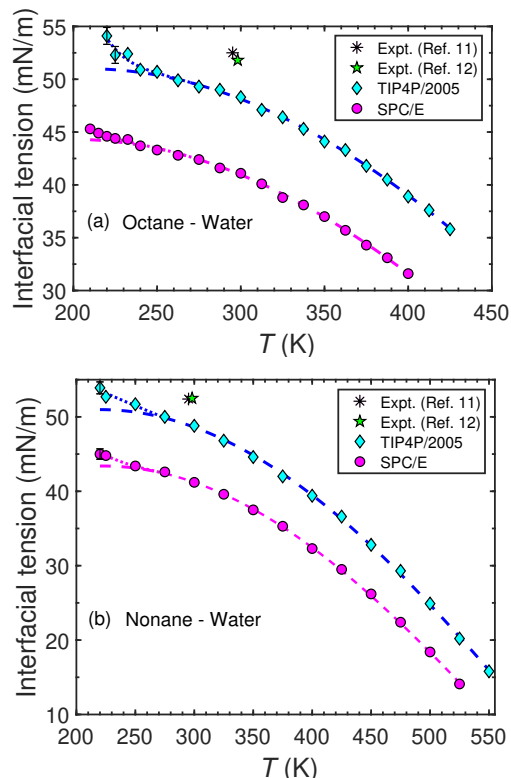

Fig. 5 Octane-water (a) and nonane-water (b) interfacial tension for PYS alkane with TIP4P/2005 water (diamonds) and SPC/E water (circles). Our results are compared with experimental alkane-water interfacial tensions (asterisk - Ref. [11], star - Ref. [12]). The dashed line represents the fitted surface tension obtained using Eq. 11, and the dotted line adds Eq. 12 to Eq. 11. The black error bars are the standard error of the mean.[98] They are shown only when they exceed the marker size. For a complete list of the standard errors, see Table S1-S4 in the ESI†.

Table 2 Parameters for the fits to the surface tension values of water and alkane-water interfacial tensions using Eq. 11 (top table) and Eq. 12 (middle table), and of the alkanes using Eq. 13 (bottom table)

Model	T_c (K)	a (mN/m)	b
SPC/E water	626.6	195.5	0.5779
TIP4P/2005 water	642.3	217.7	0.6065
SPC/E + octane	616.7	158.8	0.8132
SPC/E + nonane	617.7	166.8	0.8602
TIP4P/2005 + octane	652.2	181.2	0.8075
TIP4P/2005 + nonane	645.2	188.7	0.8350

Model	c'(mN/m)	T_a (K)	T_b (K)
SPC/E water	24.74	100.0	82.74
TIP4P/2005 water	30.00	191.5	20.00
SPC/E + octane	1.65	201.8	20.17
SPC/E + nonane	1.07	230.5	20.00
TIP4P/2005 + octane	10.00	200.6	22.10
TIP4P/2005 + nonane	10.00	158.3	83.24

Model	T_c (K)	a (mN/m)	b	c
Octane	548.3	96.77	0.8968	0.4795
Nonane	587.1	98.08	0.9243	0.5174

to the experimental values than are the SPC/E results. For the same water model, the nonane-water interfacial tension is usually slightly higher than the octane-water interfacial tension. The rate of change of interfacial tension with temperature is similar in alkane-SPC/E water and alkane-TIP4P/2005 water at higher tem-

peratures, but at lower temperatures ($T < T_s$) the interfacial tension of alkane-TIP4P/2005 water changes more rapidly than that of alkane-SPC/E water. Moreover, each of these interfacial tension curves displays a change of curvature similar to that resulting from the SIP for the pure water models. Hence, the alkane-water interfacial tension values are also fitted using Eq. 11 (dashed line in Fig. 5) and $\gamma^*(T)$ (from Eq. 12). These two fits are also added for $T \leq T_s$ to accurately account for the deviation of the interfacial tension values due to the presence of the SIP (dotted lines in Fig. 5). This deviation is notable below ≈ 250 K for alkane-SPC/E water and ≈ 275 K for alkane-TIP4P/2005 water. It is also interesting to note that while the pure alkane surface tension curves have overall positive curvature, the alkane-water interfacial tensions have generally negative curvature as do the water surface tension curves. From this behavior, we see that water has a much stronger influence than the alkane on the interfacial tension of the two liquids.

The fitting parameter values from Eqs. 11, 12, 13 are presented in Table 2.

3.2 TEMPERATURE DEPENDENT WETTING

Based on the simulation results in Section 3.1, we have calculated the spreading coefficient S for PYS octane and nonane on SPC/E water and TIP4P/2005 water and the corresponding contact angles θ_c for each of these four systems. The spreading coefficients (S) are shown in Fig. 6 and are compared to experimental results in Fig. 7. The contact angles (θ_c) are shown in Fig. 8. In Fig. 6 and Fig. 8, the filled circles and diamonds are the results obtained using the simulated interfacial tensions. The spreading coefficients, and the contact angles are found to be quite sensitive to the simulated interfacial tension values. To reduce the scatter of the simulated values, θ_c and S have also been calculated using fits to the simulated interfacial tensions, and these are represented by the dashed lines (γ_w, γ_{aw} - Eq. 11, and γ_a - Eq. 13) and the dotted lines (γ_w, γ_{aw} - Eqs. 11 + 12, and γ_a - Eq. 13). The dashed lines neglect the SIP effect in the vapor-water and the alkane-water interfacial tension curves, whereas, the dotted lines account for the SIP effect (Eq. 12).

First, let us note that the positive S values seen in Fig. 6 are consequences of our simulation methodology. According to Rowlinson and Widom,[1] initial S values may be positive for pairs of liquids that are not mutually equilibrated. In our simulations, because the mutual solubilities of alkanes and water are so low, this equilibrium condition is very difficult to satisfy given the relatively small system sizes and simulation times that are practical.

When an alkane perfectly wets water, we have $S = 0$ and $\theta_c = 0$, but for partial wetting we have $S < 0$ and $\theta_c > 0$. The behavior of each property, S and θ_c, is similar at higher temperatures for all four systems studied, but at lower temperatures, they differ for the octane-water and nonane-water systems if the effect of the SIP is neglected. Beginning at the wetting transition temperature T_w, where $S = 0$ or $\theta_c = 0$,[100] we would have perfect wetting at all higher temperatures up to the alkane critical temperature. In Table 3, T_w of each simulated alkane-water system is presented along with estimates of the experimental T_w. The estimated T_w
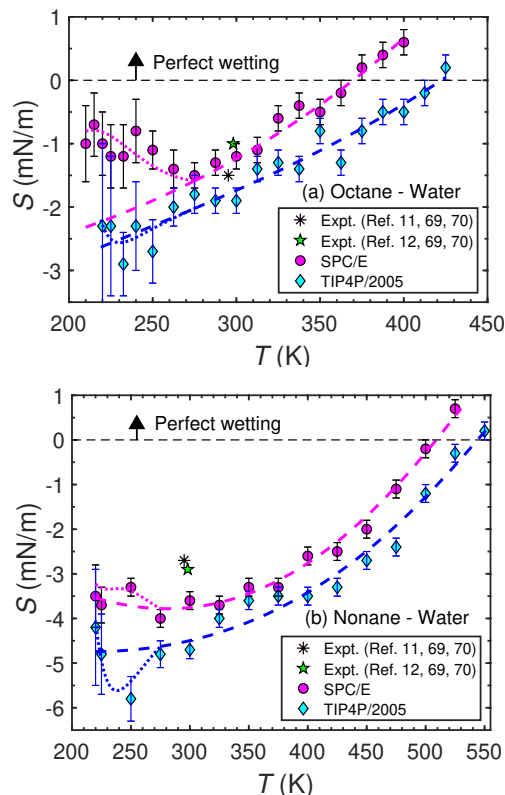

Fig. 6 Spreading coefficient (S) of (a) octane on water, and (b) nonane on water. The circles are for SPC/E water, and the diamonds are for TIP4P/2005 water. The dashed lines are obtained from fits to the simulated interfacial tension values that exclude the effect of the SIP, (Eqs. 11, 13), and the dotted lines are obtained from fits that include the SIP effect, (Eqs. 11, 12, 13). The asterisk and star represent values calculated using experimental values of the interfacial tensions from Refs 11, 12, 69 and 70. The error bars are calculated by propagating the standard errors of the mean for the surface tensions in the usual fashion as explained in the ESI†.

values for octane and nonane were obtained by extrapolating Weiss's[101] calculated T_w values for pentane, hexane and heptane as shown in the ESI†. As the temperature is reduced below T_w, partial wetting ensues and S grows increasingly more negative while θ_c increases. The S values continue to become more negative as T_s is approached.

In Fig. 7, the experimental results of Takii and Mori[45] and Akatsuka et al.[46] for S values of octane on water are compared with our simulation results. The simulated S values for octane-SPC/E water match well with the experimental values for $T < 360$ K, but they disagree markedly above 360 K. The S values for octane-TIP4P/2005 water fail to capture the trend of the experimental slopes, although they do provide better quantitative agreement in the range 380 - 420 K. The S curve for TIP4P/2005 water also agrees very well with the theoretical curve of Pham and Hirasaki.[102] The good agreement among these different approaches is likely to be coincidental in part and may be partly attributed to how we evaluate ε_{oc}.

Above 360 K, the experimental S values increase much more slowly as S tends toward zero at 484 K (by linear extrapolation of the high temperature points), a value somewhat higher than
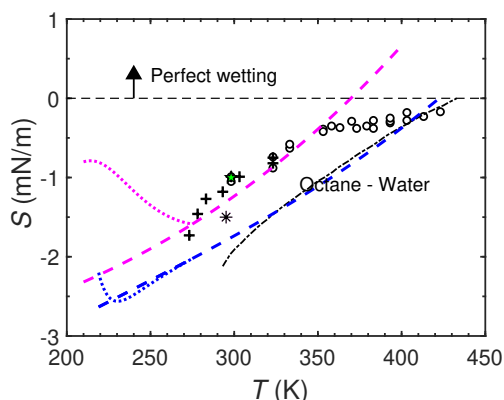
Fig. 7 Spreading coefficient S of octane-water, shown in Fig. 6 (a), compared with experimental results [45,46] (markers) and with a theoretical calculation [102] (dash-dotted line). The circles are the values determined by Akatsuka et al., [46] and the plus signs ($+$) are the values determined by Takii and Mori [45] as corrected by Akatsuka et al. [46] for possible bias errors. The asterisk and star represent values calculated using experimental values of the interfacial tensions from Refs. 11, 12, 69 and 70. The dashed and dotted lines are the same as those in Fig. 6 (a).

Table 3 Wetting transition temperatures, T_w, for PYS alkanes on water from MD simulations, theoretical calculations and experimental estimates.

Alkane	Model / Theory / Experiment	T_w (K)
Octane	SPC/E water	370$\pm$4
Nonane	SPC/E water	509$\pm$5
Octane	TIP4P/2005 water	423$\pm$6
Nonane	TIP4P/2005 water	545$\pm$3
Octane	Water-Experiment	484[†]
Octane	Hamaker-Lifshitz theory	433[‡]
Nonane	Hamaker-Lifshitz theory	469[‡]
Octane	Water-Estimated	457[*]
Nonane	Water-Estimated	500[*]

[†] by linearly extrapolating the high T data shown in Fig. 7.
[‡] Ref. [102].
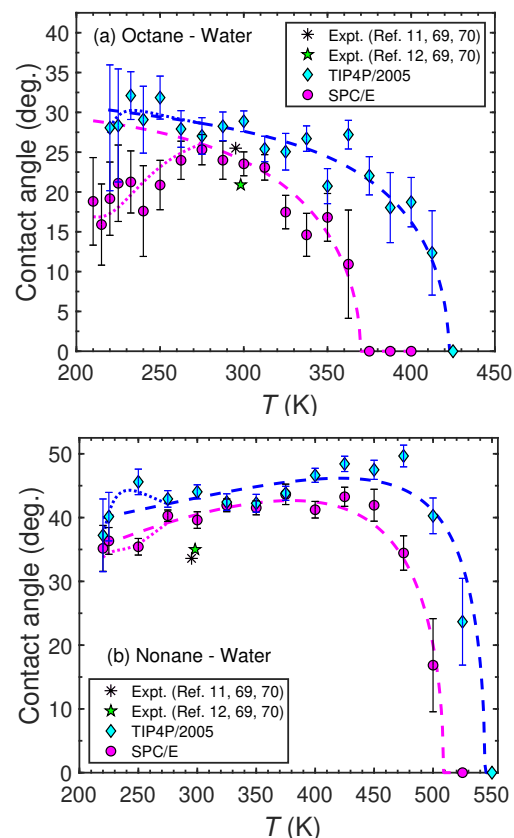[*] by extrapolating results from Ref. [101]. See Fig. S9 in the ESI[†].

Fig. 8 The contact angle formed by octane on water (a) and nonane on water (b). The diamonds are for TIP4P/2005 water, and the circles are for SPC/E water. The dashed lines are obtained from fits to the simulated interfacial tension values that exclude the effect of the SIP, (Eqs. 11, 13), and the dotted lines are obtained from fits that include the SIP effect, (Eqs. 11, 12, 13). The asterisk and star represent values calculated using experimental values of the interfacial tensions from Refs. 11, 12, 69 and 70. The error bars are calculated by propagating the standard errors of the mean for the surface tensions in the usual fashion as explained in the ESI[†].

the other estimated values in Table 3. A likely reason for the high temperature discrepancies is our method of determining the surface tension of the liquids. As mentioned earlier, unlike in a real system, our simulations are for pure liquids that are not mutually equilibrated, so our S values are likely to be initial, and not equilibrium values.

The obvious reason for the discrepancy between the two sets of simulation results is the difference in the quantity $\delta_{aw} = \gamma_w - \gamma_{aw}$ for the two water models. Considering that TIP4P/2005 water gives better results for both γ_w and γ_{aw} than does SPC/E water (c.f. Fig. 3 and Fig. 5), it surprised us to see that the SPC/E model produced better results for S. In the ESI[†], we compare the values of δ_{aw} for each water model for both alkanes. What we see is that δ_{aw} is consistently slightly smaller for TIP4P/2005 so that when γ_a is subtracted from each δ_{aw} value, we obtain the observed trend in S values. It is worth noting that values of S are consistently much smaller than the individual interfacial tension values, and we are thus in the notoriously difficult situation of trying to precisely determine a small number by taking the difference of two large numbers, γ_w and ($\gamma_{aw} + \gamma_a$). Nevertheless, despite the

poorer predicted slope of S versus T for TIP4P/2005, the S values for this model generally differ by less than 0.6 mN/m from the experimental values, and the simulated wetting transition temperature is much more realistic than that for SPC/E water.

Below T_s, when the effect of the SIP is excluded in the interfacial tensions, S continues to decrease as T decreases except for nonane-SPC/E water as seen by the low T portion of the dashed line in Fig. 6 (b). However, the SPC/E and TIP4P/2005 water models do exhibit the SIP in the surface tension curve, and this is also reflected in the alkane-water interfacial tension curves. When the SIP effect is taken into account, S deviates generally towards less negative values with decreasing temperatures, although for nonane-TIP4P/2005 water the increase of S is first preceded by a further decrease. This increasing behavior of S begins at T_s for alkane-SPC/E water, and below T_m of TIP4P/2005 water for alkane-TIP4P/2005 water.

In Figure 8, we see that the temperature dependence of θ_c for octane on water differs from that of nonane on water. Just below T_w, the contact angle in all systems initially shows a normal increasing trend with decreasing temperature. For octane-SPC/E

water, this normal trend continues down to T_s. Below T_s, the low temperature extrapolation of the high temperature ($T \geq T_s$) fit to the interfacial tension predicts this normal trend (see dashed line for $T \leq T_s$ in Fig. 8(a)). In contrast, the contact angle calculated using the simulated interfacial tension values (circles) as well as the fits to the interfacial tension values for the full temperature range (dotted line) shows a trend reversal: θ_c begins to decrease, as if the system were approaching a low temperature transition to perfect wetting. For octane-TIP4P/2005 water, such a reversal might also occur near 230 K, although given the relatively large uncertainties for the two lowest temperature points one could equally argue for no trend reversal.

For nonane-water, the reversal trend of contact angle occurs at comparatively high temperatures (roughly 375 K for SPC/E water and 450 K for TIP4P/2005 water). Unlike in the octane-water system, the SIP has no significant effect on the contact angle in the nonane-water systems. Although, the contact angle decreases with decreasing temperature in the nonane-water system at lower temperatures, the perfect wetting at lower temperature could not be realized because surface freezing occured in the liquid-vapor simulation of PYS nonane at 215 K.

The decreasing trend of contact angle with decreasing temperature observed in Fig. 8 is highly unusual. To the best of our knowledge, such behavior has not yet been reported for a bulk system of two liquids with limited miscibility and no lower consolute temperature. On the other hand, this unusual low temperature wetting behavior is consistent with behavior seen in the previous study of wetting on nanodroplets.[54]

In the nonane-water systems, S and θ_c are not correlated in the partial wetting state although they are correlated in the octane-water systems. In the octane-water systems, starting from the lowest temperature, as T increases, the decreasing S values (see dotted line in Fig. 6 (a)) correspond to increasing θ_c values (see dotted line in Fig. 8 (a)). Above T_s, as S increases, θ_c decreases until the systems approach the perfect wetting state where both S and θ_c equal zero. However, such a correlation is not observed in nonane-water systems for partial wetting states, except near the wetting transition at higher temperatures. Instead S is seen to be a double valued function of θ_c. For example, for nonane-SPC/E water, at $\theta_c = 39.2°$, two different S values are found: -3.8 mN/m and -1.8 mN/m at temperatures 275 K and 448 K, respectively.

Next, we briefly examine the sensitivity of the results to the value of the LJ cross interaction parameter ε_{oc}. As we see in Fig. 9, because the liquid-liquid interfacial tension is quite sensitive to this value, the contact angle shows a similar sensitivity. For PYS nonane-SPC/E water, the interfacial tension and the contact angle are found to be decreased by $\sim$2% and $\sim$13%, respectively, at 300 K by increasing ε_{oc} from 0.65 kJ/mol to 0.66 kJ/mol, while keeping σ_{oc} constant. With ε_{oc}=0.66 kJ/mol, the contact angle formed by nonane on the water is found to match nearly perfectly with that calculated using experimental interfacial tension values.

We also see in Fig. 9 the importance of the tail correction γ_t on the wetting behavior. The contact angles formed by nonane on SPC/E water are represented by open squares when the tail correction γ_t is not included in the interfacial tension and by filled squares when it is. For $T \leq 250$ K, when γ_t is excluded from
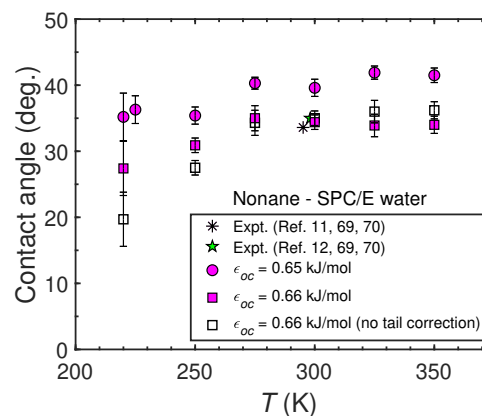

Fig. 9 The contact angles formed at different temperatures by nonane on SPC/E water when ε_{oc}=0.65 kJ/mol (circles) and ε_{oc}=0.66 kJ/mol (squares). Filled markers represent contact angles calculated using simulated interfacial tensions. Open squares are the counter-part of the filled squares without long-range tail corrections to the interfacial tensions. The asterisk and star represent values calculated using experimental values of the interfacial tensions from Refs. 11, 12, 69 and 70. The error bars are calculated by propagating the standard errors of the mean for the surface tensions in the usual fashion as explained in the ESI[†].

the interfacial tensions, the contact angle decreases rapidly, and can be extrapolated to a wetting transition at a lower T ($<$ 210 K). The tail-corrected values also decrease, but they extrapolate to a wetting transition at an even lower T. These hypothetical transition temperatures are lower than the melting temperature for either SPC/E water or nonane.

4   Conclusions

Using molecular dynamics simulations, we have studied the surface tension of SPC/E and TIP4P/2005 water, PYS alkanes (octane, nonane), and the corresponding alkane-water interfacial tensions to explore the temperature dependent wetting behavior of these alkanes on water.

In the low temperature region ($T < 275$ K), the surface tensions of the SPC/E and TIP4P/2005 water models are found to increase more rapidly with decreasing temperature, thereby showing the presence of the SIP, as found by others,[87,93] in the surface tension curves. We also simulated the temperature dependent behavior of the interfacial tensions for PYS alkane (octane, nonane) and SPC/E or TIP4P/2005 water by choosing values for the LJ cross-interaction parameters ε_{oc} and σ_{oc} between unlike atoms that would yield values for the spreading coefficient S relatively close to the values determined from experimental surface tension values near 300 K. The presence of the SIP is also reflected in the alkane-water interfacial tension (γ_{aw}). There is a change in curvature in the γ_{aw} curves at lower temperatures for both water models, such that the interfacial tension increases more rapidly with decreasing temperature below $\approx$250 K for SPC/E water and $\approx$275 K for TIP4P/2005 water. The overall behavior of these curves is dominated by the water model behavior.

Using the simulated interfacial tension values, PYS octane was found to perfectly wet both SPC/E water and TIP4P/2005 water at high temperature (370 K for SPC/E and 423 K for TIP4P/2005 based on either S=0 or θ_c=0). The simulated transition temper-

atures are somewhat lower than our estimates of 457 K or 484 K for the experimental value, although the value for TIP4P/2005 water is close to the Hamaker-Lifshitz theory prediction of 433 K by Pham and Hirasaki.[102] PYS nonane behaved similarly to octane on both water models, yielding appropriately larger wetting transition temperatures. These values are 509 K for SPC/E water and 545 K for TIP4P/2005 water in comparision to 500 K estimated for the real nonane-water system and 469 K based on Hamaker-Lifshitz theory.[102]

Below T_w, S and θ_c for the octane-water system are strongly correlated: θ_c increases as S decreases and vice versa. Such a correlation holds only near T_w for the nonane-water system. At lower temperatures, S is instead a doubled valued function of θ_c. The nonane-water systems also exhibit an unusual temperature dependence of θ_c at lower temperatures, in which the contact angle decreases with a decrease in temperature. The wetting behavior of the nonane-water system is not affected significantly by the presence of the SIP in the interfacial tension curves.

In contrast, for octane-water the wetting behavior is strongly influenced by the SIP, particularly for SPC/E water. The role of the SIP is to enhance the just described unusual temperature dependence of the contact angle. This unusual behavior starts to occur at T_s for octane-SPC/E water, but for octane-TIP4P/2005 water it is delayed until well into the supercooled water region ($<$ 249 K). This unusual temperature dependent behavior for octane would not occur if there were no SIP in the interfacial tension curves. If carried to sufficiently low temperatures, this behavior might lead to a transition to perfect wetting at a very low temperature in the octane-SPC/E water system. The wetting behavior depends on the competing rates of change of the water surface tension and the alkane-water interfacial tension with temperature. When γ_w is dominant, δ_{aw} ($=\gamma_w - \gamma_{aw}$) increases, S increases and θ_c decreases; when γ_{aw} is dominant, the reverse occurs and normal behavior is observed.

The occurrence of low temperature perfect wetting of alkanes on water might occur if γ_w were to increase faster than γ_{aw} with decreasing temperature below the SIP. While a low temperature wetting transition might be inferred from the octane-SPC/E water simulation results that include the SIP effect, our simulations did not go to low enough temperatures to confirm this. Previously, the unusual positive correlation of the contact angle with temperature formed by nonane on SPC/E water was also observed in nanodroplet simulations in which the geometric mean approach was used to determine the LJ energy parameter between unlike atoms.[54] So this unusual feature has now been found twice for two different combining rules to determine the strength of the cross interaction paramenter, ε_{oc}. While the idea of a low temperature transition to perfect wetting in alkane-water systems is intriguing, our simulations did not extend to low enough temperatures to confirm this for our model systems.

The degree to which we can trust the low temperature wetting behavior predicted by these simulations remains an open question. Given that the SIP may significantly affect the wetting behavior, it is encouraging that both water models predict the SIP. On the other hand, neither water model predicts very well the location of the SIP, which lies in the deeply supercooled region

for real water. The SIP of SPC/E water lies in its stable liquid region while that of TIP4P/2005 is in its slightly supercooled region. Based on our results, we feel that the low temperature wetting behavior of organic liquids on water is deserving of much further theoretical and experimental study.

Conflicts of interest

There are no conflicts to declare.

Acknowledgements

Notes and references

1 J. S. Rowlinson and B. Widom, *Molecular Theory of Capillarity*, Dover Publications, Inc., Mineola NY, 2002.

2 K. Ragil, D. Bonn, D. Broseta, J. Indekeu, F. Kalaydjian and J. Meunier, *J. Petrol. Sci. Eng.*, 1998, **20**, 177–183.

3 D. Bonn, E. Bertrand, N. Shahidzadeh, K. Ragil, H. T. Dobbs, A. I. Posazhennikova, D. Broseta, J. Meunier and J. O. Indekeu, *J. Phys. Condens. Matter*, 2001, **13**, 4903.

4 V. C. Weiss, *Fluid Ph. Equilibria*, 2007, **256**, 145–150.

5 P. A. Ash, C. D. Bain and H. Matsubara, *Curr. Opin. Colloid Interface Sci.*, 2012, **17**, 196–204.

6 J. W. Gibbs, *The Scientific Papers of J. Willard Gibbs, Volume One Thermodynamics*, Dover Publications, Inc., New York, 1961, p. 258.

7 F. Hauxwell and R. H. Ottewill, *J. Colloid Interface Sci.*, 1970, **34**, 473–479.

8 C. Jho, D. Nealon, S. Shogbola and A. D. King Jr, *J. Colloid Interface Sci.*, 1978, **65**, 141–154.

9 H. Matsubara, M. Murase, Y. H. Mori and A. Nagashima, *Int. J. Thermophys.*, 1988, **9**, 409–424.

10 F. Hauxwell, N. R. Pallas and B. A. Pethica, *Langmuir*, 1992, **8**, 602–603.

11 A. Goebel and K. Lunkenheimer, *Langmuir*, 1997, **13**, 369–372.

12 D. M. Mitrinović, A. M. Tikhonov, M. Li, Z. Huang and M. L. Schlossman, *Phys. Rev. Lett.*, 2000, **85**, 582.

13 D. J. Donahue and F. E. Bartell, *J. Phys. Chem.*, 1952, **56**, 480–484.

14 S. J. Rehfeld, *J. Phys. Chem.*, 1967, **71**, 738–745.

15 R. Aveyard and D. A. Haydon, *Trans. Faraday Soc.*, 1965, **61**, 2255–2261.

16 Y. H. Mori, N. Tsui and M. Kiyomiya, *J. Chem. Eng. Data*, 1984, **29**, 407–412.

17 S. Zeppieri, J. Rodríguez and A. L. López de Ramos, *J. Chem. Eng. Data*, 2001, **46**, 1086–1088.

18 F. Biscay, A. Ghoufi and P. Malfreyt, *Phys. Chem. Chem. Phys.*, 2011, **13**, 11308–11316.

19 P. Naeiji, T. K. Woo, S. Alavi, F. Varaminian and R. Ohmura, *J. Chem. Phys.*, 2019, **150**, 114703.

20 C. Vega and E. de Miguel, *J. Chem. Phys.*, 2007, **126**, 154707.

21 R. Sakamaki, A. K. Sum, T. Narumi and K. Yasuoka, *J. Chem. Phys.*, 2011, **134**, 124708.

22 A. E. Ismail, M. Tsige, P. J. Veld In 't and G. S. Grest, *Mol. Phys.*, 2007, **105**, 3155–3163.

23 C. Ibergay, A. Ghoufi, F. Goujon, P. Ungerer, A. Boutin, B. Rousseau and P. Malfreyt, *Phys. Rev. E*, 2007, **75**, 051602.

24 F. N. Mendoza, R. López-Rendón, J. López-Lemus, J. Cruz and J. Alejandre, *Mol. Phys.*, 2008, **106**, 1055–1059.

25 M. A. Amat and G. C. Rutledge, *J. Chem. Phys.*, 2010, **132**, 114704.

26 S. Braun, A. R. Imre and T. Kraska, *J. Chem. Phys.*, 2013, **138**, 244710.

27 D. A. Hernandez and H. Domínguez, *J. Chem. Phys.*, 2013, **138**, 134702.

28 E. Galicia-Andrés and M. Medeiros, *J. Mol. Liq.*, 2017, **248**, 253–263.

29 T. R. Underwood and H. C. Greenwell, *Sci. Rep.*, 2018, **8**, 1–11.

30 A. R. van Buuren, S.-J. Marrink and H. J. C. Berendsen, *J. Phys. Chem.*, 1993, **97**, 9206–9212.

31 Y. Zhang, S. E. Feller, B. R. Brooks and R. W. Pastor, *J. Chem. Phys.*, 1995, **103**, 10252–10266.

32 J. L. Rivera, C. McCabe and P. T. Cummings, *Phys. Rev. E*, 2003, **67**, 011603.

33 H. A. Patel, E. B. Nauman and S. Garde, *J. Chem. Phys.*, 2003, **119**, 9199–9206.

34 S. S. Jang, S.-T. Lin, P. K. Maiti, M. Blanco, W. A. Goddard, P. Shuler and Y. Tang, *J. Phys. Chem. B*, 2004, **108**, 12130–12140.

35 J. P. Nicolas and N. R. de Souza, *J. Chem. Phys.*, 2004, **120**, 2464–2469.

36 H. Xiao, Z. Zhen, H. Sun, X. Cao, Z. Li, X. Song, X. Cui and X. Liu, *Sci. China Chem.*, 2010, **53**, 945–949.

37 M. Kunieda, Y. Liang, Y. Fukunaka, T. Matsuoka, K. Takamura, N. Loahardjo, W. Winoto and N. R. Morrow, *Energy Fuels*, 2012, **26**, 2736–2741.

38 C. Zhang and P. Carloni, *J. Phys. Condens. Matter*, 2012, **24**, 124109.

39 J.-C. Neyt, A. Wender, V. Lachet, A. Ghoufi and P. Malfreyt, *J. Chem. Theory Comput.*, 2014, **10**, 1887–1899.

40 Y. Ghadar and A. E. Clark, *Phys. Chem. Chem. Phys.*, 2014, **16**, 12475–12487.

41 Y. Qiu and V. Molinero, *Crystals*, 2017, **7**, 86.

42 G. Rucker, X. Yu and L. Zhang, *Fuel*, 2020, **267**, 117252.

43 K. Ragil, J. Meunier, D. Broseta, J. O. Indekeu and D. Bonn, *Phys. Rev. Lett.*, 1996, **77**, 1532.

44 E. Bertrand, H. Dobbs, D. Broseta, J. Indekeu, D. Bonn and J. Meunier, *Phys. Rev. Lett.*, 2000, **85**, 1282.

45 T. Takii and Y. H. Mori, *J. Colloid Interface Sci.*, 1993, **161**, 31–37.

46 S.-Y. Akatsuka, H. Yoshigiwa and Y. H. Mori, *J. Colloid Interface Sci.*, 1995, **172**, 335–340.

47 N. Shahidzadeh, D. Bonn, K. Ragil, D. Broseta and J. Meunier, *Phys. Rev. Lett.*, 1998, **80**, 3992.

48 S. Rafaï, D. Bonn, E. Bertrand, J. Meunier, V. C. Weiss and J. O. Indekeu, *Phys. Rev. Lett.*, 2004, **92**, 245701.

49 V. C. Weiss and B. Widom, *Physica A*, 2001, **292**, 137–145.

50 V. C. Weiss and J. O. Indekeu, *Fluid Ph. Equilibria*, 2004, **222**, 269–274.

51 V. C. Weiss, E. Bertrand, S. Rafaï, J. O. Indekeu and D. Bonn, *Phys. Rev. E*, 2007, **76**, 051602.

52 L. Boinovich and A. Emelyanenko, *J. Phys. Chem. B*, 2007, **111**, 10217–10223.

53 L. Boinovich and A. Emelyanenko, *Adv. Colloid Interface Sci.*, 2009, **147**, 44–55.

54 F. Hrahsheh and G. Wilemski, in *Nucleation and Atmospheric Aerosols*, ed. P. J. DeMott and C. D. O'Dowd, AIP Conference Proceedings 1527, AIP Publishing, Melville, New York, 2013, pp. 63–66.

55 D. W. Pohl and W. I. Goldburg, *Phys. Rev. Lett.*, 1982, **48**, 1111.

56 H. T. Davis, *Statistical Mechanics of Phases, Interfaces, and Thin Films*, Wiley-VCH, 1996.

57 V. Vinš, J. Hykl, J. Hrubỳ, A. Blahut, D. Celný, M. Čenskỳ and O. Prokopová, *J. Phys. Chem. Lett.*, 2020, **11**, 4443–4447.

58 W. Paul, D. Y. Yoon and G. D. Smith, *J. Chem. Phys.*, 1995, **103**, 1702–1709.

59 N. Waheed, M. S. Lavine and G. C. Rutledge, *J. Chem. Phys.*, 2002, **116**, 2301–2309.

60 N. Waheed, M. J. Ko and G. C. Rutledge, *Polymer*, 2005, **46**, 8689–8702.

61 P. Yi and G. C. Rutledge, *J Chem. Phys.*, 2009, **131**, 134902.

62 V. P. Modak, H. Pathak, M. Thayer, S. J. Singer and B. E. Wyslouzil, *Phys. Chem. Chem. Phys.*, 2013, **15**, 6783–6795.

63 V. P. Modak, B. E. Wyslouzil and S. J. Singer, *J. Chem. Phys.*, 2020, **153**, 224501.

64 H. J. C. Berendsen, J. R. Grigera and T. P. Straatsma, *J. Phys. Chem.*, 1987, **91**, 6269–6271.

65 J. L. Abascal and C. Vega, *J. Chem. Phys.*, 2005, **123**, 234505.

66 The expression for the torsional potential (V_t) in Eq. (4) is the standard formulation assuming $\phi = 0°$ in the trans conformation. In the LAMMPS convention, the trans conformation corresponds to $\phi = 180°$, so the equation for V_t must be adjusted accordingly.

67 H. A. Lorentz, *Annalen der Physik*, 1881, **248**, 127–136.

68 D. Berthelot, *Compt. Rendus*, 1898, **126**, 1703–1706.

69 T. Petrova and R. B. Dooley, *Revised Release on Surface Tension of Ordinary Water Substance*, International Association for the Properties of Water and Steam (IAPWS), Moscow, Russia, 2014.

70 E. W. Lemmon, M. O. McLinden and D. G. Friend, "Thermophysical Properties of Fluid Systems", in *NIST Chemistry WebBook, NIST Standard Reference Database Number 69*, ed.

P. J. Linstrom and W. G. Mallard, National Institute of Standards and Technology, Gaithersburg MD, 20899, 2020.

71 L. Martínez, R. Andrade, E. G. Birgin and J. M. Martínez, *J. Comput. Chem.*, 2009, **30**, 2157–2164.

72 A. I. Jewett, Z. Zhuang and J.-E. Shea, *Biophys. J.*, 2013, **104**, 169a.

73 S. Plimpton, *J. Comput. Phys.*, 1995, **117**, 1–19.

74 A. Ghoufi, P. Malfreyt and D. J. Tildesley, *Chem. Soc. Rev.*, 2016, **45**, 1387–1409.

75 W. C. Swope, H. C. Andersen, P. H. Berens and K. R. Wilson, *J. Chem. Phys.*, 1982, **76**, 637–649.

76 S. Nosé, *J. Chem. Phys.*, 1984, **81**, 511–519.

77 W. G. Hoover, *Phys. Rev. A*, 1985, **31**, 1695.

78 M. Parrinello and A. Rahman, *J. Appl. Phys.*, 1981, **52**, 7182–7190.

79 J.-P. Ryckaert, G. Ciccotti and H. J. C. Berendsen, *J. Comput. Phys.*, 1977, **23**, 327–341.

80 R. W. Hockney and J. W. Eastwood, *Computer Simulation using Particles*, Adam Hilger, Bristol, 1989.

81 G. A. Chapela, G. Saville, S. M. Thompson and J. S. Rowlinson, *J. Chem Soc. Faraday Trans. II*, 1977, **73**, 1133–1144.

82 E. M. Blokhuis, D. Bedeaux, C. D. Holcomb and J. A. Zollweg, *Mol. Phys.*, 1995, **85**, 665–669.

83 Z. Li, F. Yuan, K. A. Fichthorn, S. T. Milner and R. G. Larson, *Macromolecules*, 2014, **47**, 6441–6452.

84 L. Lundberg and O. Edholm, *J. Chem. Theory Comput.*, 2016, **12**, 4025–4032.

85 K. Abe, T. Sumi and K. Koga, *J. Chem. Phys.*, 2014, **141**, 18C516.

86 A. Haji-Akbari and P. G. Debenedetti, *Proc. Natl. Acad. Sci. U. S. A.*, 2017, **114**, 3316–3321.

87 X. Wang, K. Binder, C. Chen, T. Koop, U. Pöschl, H. Su and Y. Cheng, *Phys. Chem. Chem. Phys.*, 2019, **21**, 3360–3369.

88 P. T. Hacker, *Experimental Values of the Surface Tension of Supercooled Water*, National Advisory Committee for Aeronautics, Washington, 1951.

89 V. Holten, D. G. Labetski and M. E. H. van Dongen, *J. Chem. Phys.*, 2005, **123**, 104505.

90 J. Hrubỳ, V. Vinš, R. Mareš, J. Hykl and J. Kalová, *J. Phys. Chem. Lett.*, 2014, **5**, 425–428.

91 V. Vinš, M. Fransen, J. Hykl and J. Hrubỳ, *J. Phys. Chem. B*, 2015, **119**, 5567–5575.

92 V. Vinš, J. Hošek, J. Hykl and J. Hrubỳ, *J. Chem. Eng. Data*, 2017, **62**, 3823–3832.

93 Y. J. Lü and B. Wei, *Appl. Phys. Lett.*, 2006, **89**, 164106.

94 V. Vinš, D. Celnỳ, B. Planková, T. Němec, M. Duška and J. Hrubỳ, *EPJ Web Conf.*, 2016, **114**, 02136.

95 M. Sega and C. Dellago, *J. Phys. Chem. B*, 2017, **121**, 3798–3803.

96 A. E. Ismail, G. S. Grest and M. J. Stevens, *J. Chem. Phys.*, 2006, **125**, 014702.

97 F. Chen and P. E. Smith, *J. Chem. Phys.*, 2007, **126**, 221101.

98 D. G. Altman and J. M. Bland, *BMJ*, 2005, **331**, 903.

99 T. Klein, S. Yan, J. Cui, J. W. Magee, K. Kroenlein, M. H. Rausch, T. M. Koller and A. P. Fröba, *J. Chem. Eng. Data*, 2019, **64**, 4116–4131.

100 As shown in Rowlinson and Widom (Ref. 1), Eq. (2) can also be written as $\cos\theta_c = 1 + S(\gamma_w + \gamma_a + \gamma_{aw})/(2\gamma_a\gamma_{aw})$. Thus, when $S = 0$, it follows directly that $\theta_c = 0$.

101 V. C. Weiss, *J. Chem. Phys.*, 2006, **125**, 084718.

102 D. T.-K. Pham and G. J. Hirasaki, *J. Petrol. Sci. Eng.*, 1998, **20**, 239–246.